Nanoparticles for highly efficient multiphoton fluorescence bioimaging

Laura Martinez Maestro,[1] Emma Martín Rodriguez,[1] Fiorenzo Vetrone,[2] Rafik Naccache,[2] Hector Loro Ramirez,[3] Daniel Jaque,[1] John A. Capobianco,[2,4] and José García Solé[1,*]

[1]GIEL, Departamento de Física de Materiales, Universidad Autónoma de Madrid, 8049 Madrid, Spain
[2]Department of Chemistry and Biochemistry, Concordia University, H4B 1R6, Montreal, Canada
[3]Facultad de Ciencias, Universidad Nacional de Ingeniería, P.O. Box 31-139, Lima, Perú
[4]capo@vax2.concordia.ca
**jose.garcia_sole@uam.es*

Abstract: In this paper, we demonstrate for the first time that the new class of fluoride-based inorganic upconverting nanoparticles, $NaYF_4$:Er^{3+}, Yb^{3+}, are the most efficient multiphoton excited fluorescent nanoparticles developed to date. The near-infrared-to-visible conversion efficiency of the aforementioned nanoparticles surpasses that of CdSe quantum dots and gold nanorods, which are the commercially available inorganic fluorescent nanoprobes presently used for multiphoton fluorescence bioimaging. The results presented here open new perspectives for the implementation of fluorescence tomography by multiphoton fluorescence imaging.

OCIS codes: (300.0300) Spectroscopy; (160.4236) Nanomaterials; (170.2520) Fluorescence Microscopy; (170.3880) Medical and biological imaging.

References and links

1. I. L. Medintz, H. T. Uyeda, E. R. Goldman, and H. Mattoussi, "Quantum dot bioconjugates for imaging, labelling and sensing," Nat. Mater. **4**(6), 435–446 (2005).
2. X. Gao, Y. Cui, R. M. Levenson, L. W. K. Chung, and S. Nie, "*In vivo* cancer targeting and imaging with semiconductor quantum dots," Nat. Biotechnol. **22**(8), 969–976 (2004).
3. M. Bruchez, Jr., M. Moronne, P. Gin, S. Weiss, and A. P. Alivisatos, "Semiconductor nanocrystals as fluorescent biological labels," Science **281**(5385), 2013–2016 (1998).
4. H. Wang, T. B. Huff, D. A. Zweifel, W. He, P. S. Low, A. Wei, and J.-X. Cheng, "*In vitro* and *in vivo* two-photon luminescence imaging of single gold nanorods," Proc. Natl. Acad. Sci. U.S.A. **102**(44), 15752–15756 (2005).
5. D. R. Larson, W. R. Zipfel, R. M. Williams, S. W. Clark, M. P. Bruchez, F. W. Wise, and W. W. Webb, "Water-soluble quantum dots for multiphoton fluorescence imaging in vivo," Science **300**(5624), 1434–1436 (2003).
6. K. König, "Multiphoton microscopy in life sciences," J. Microsc. **200**(Pt 2), 83–104 (2000).
7. S. Mulligan, and B. MacVicar, "Two-photon fluorescence microscopy: basic principles, advantages and risks," in *Modern Research and Educational Topics in Microscopy*, A. Méndez-Vilas, and J. Díaz, eds. (FORMATEX, Badajoz, Spain, 2007), pp. 881–889.
8. N. Chanda, R. Shukla, K. V. Katti, and R. Kannan, "Gastrin releasing protein receptor specific gold nanorods: breast and prostate tumor avid nanovectors for molecular imaging," Nano Lett. **9**(5), 1798–1805 (2009).
9. N. J. Durr, T. Larson, D. K. Smith, B. A. Korgel, K. Sokolov, and A. Ben-Yakar, "Two-photon luminescence imaging of cancer cells using molecularly targeted gold nanorods," Nano Lett. **7**(4), 941–945 (2007).
10. X. Huang, I. H. El-Sayed, W. Qian, and M. A. El-Sayed, "Cancer cell imaging and photothermal therapy in the near-infrared region by using gold nanorods," J. Am. Chem. Soc. **128**(6), 2115–2120 (2006).
11. X. Huang, S. Neretina, and M. A. El-Sayed, "Gold nanorods: from synthesis and properties to biological and biomedical applications," Adv. Mater. **21**(48), 4880–4910 (2009).
12. H. Kang, B. Jia, J. Li, D. Morrish, and M. Gu, "Enhanced photothermal therapy assisted with gold nanorods using a radially polarized beam," Appl. Phys. Lett. **96**(6), 063702 (2010).
13. S. Eustis, and M. El-Sayed, "Aspect ratio dependence of the enhanced fluorescence intensity of gold nanorods: experimental and simulation study," J. Phys. Chem. B **109**(34), 16350–16356 (2005).
14. M. Steiner, C. Debus, A. V. Failla, and A. J. Meixner, "Plasmon-enhanced emission in gold nanoparticle aggregates," J. Phys. Chem. C **112**(8), 3103–3108 (2008).
15. L. Tong, Q. Wei, A. Wei, and J.-X. Cheng, "Gold nanorods as contrast agents for biological imaging: optical properties, surface conjugation and photothermal effects," Photochem. Photobiol. **85**(1), 21–32 (2009).

#132348 - $15.00 USD Received 27 Jul 2010; revised 24 Sep 2010; accepted 26 Sep 2010; published 26 Oct 2010

16. D.-S. Wang, F.-Y. Hsu, and C.-W. Lin, "Surface plasmon effects on two photon luminescence of gold nanorods," Opt. Express **17**(14), 11350–11359 (2009).
17. C. J. Murphy, A. M. Gole, J. W. Stone, P. N. Sisco, A. M. Alkilany, E. C. Goldsmith, and S. C. Baxter, "Gold nanoparticles in biology: beyond toxicity to cellular imaging," Acc. Chem. Res. **41**(12), 1721–1730 (2008).
18. D. K. Chatterjee, A. J. Rufaihah, and Y. Zhang, "Upconversion fluorescence imaging of cells and small animals using lanthanide doped nanocrystals," Biomaterials **29**(7), 937–943 (2008).
19. N. M. Idris, Z. Li, L. Ye, E. K. W. Sim, R. Mahendran, P. C.-L. Ho, and Y. Zhang, "Tracking transplanted cells in live animal using upconversion fluorescent nanoparticles," Biomaterials **30**(28), 5104–5113 (2009).
20. Y. I. Park, J. H. Kim, K. T. Lee, K.-S. Jeon, H. B. Na, J. H. Yu, H. M. Kim, N. Lee, S. H. Choi, S.-I. Baik, H. Kim, S. P. Park, B.-J. Park, Y. W. Kim, S. H. Lee, S.-Y. Yoon, I. C. Song, W. K. Moon, Y. D. Suh, and T. Hyeon, "Nonblinking and nonbleaching upconverting nanoparticles as an optical imaging nanoprobe and T1 magnetic resonance imaging contrast agent," Adv. Mater. **21**(44), 4467–4471 (2009).
21. S. Jiang, Y. Zhang, K. M. Lim, E. K. W. Sim, and L. Ye, "NIR-to-visible upconversion nanoparticles for fluorescent labeling and targeted delivery of siRNA," Nanotechnology **20**(15), 155101 (2009).
22. M. Wang, C.-C. Mi, W.-X. Wang, C.-H. Liu, Y.-F. Wu, Z.-R. Xu, C.-B. Mao, and S.-K. Xu, "Immunolabeling and NIR-excited fluorescent imaging of HeLa cells by using $NaYF_4$:Yb,Er upconversion nanoparticles," ACS Nano **3**(6), 1580–1586 (2009).
23. L. Xiong, Z. Chen, Q. Tian, T. Cao, C. Xu, and F. Li, "High contrast upconversion luminescence targeted imaging in vivo using peptide-labeled nanophosphors," Anal. Chem. **81**(21), 8687–8694 (2009).
24. M. Yu, F. Li, Z. Chen, H. Hu, C. Zhan, H. Yang, and C. Huang, "Laser scanning up-conversion luminescence microscopy for imaging cells labeled with rare-earth nanophosphors," Anal. Chem. **81**(3), 930–935 (2009).
25. J. Zhou, Y. Sun, X. Du, L. Xiong, H. Hu, and F. Li, "Dual-modality *in vivo* imaging using rare-earth nanocrystals with near-infrared to near-infrared (NIR-to-NIR) upconversion luminescence and magnetic resonance properties," Biomaterials **31**(12), 3287–3295 (2010).
26. G. Yi, H. Lu, S. Zhao, Y. Ge, W. Yang, D. Chen, and L.-H. Guo, "Synthesis, characterization, and biological application of size-controlled nanocrystalline $NaYF_4$: Yb,Er infrared-to-visible up-conversion phosphors," Nano Lett. **4**(11), 2191–2196 (2004).
27. F. Vetrone, R. Naccache, A. Juarranz de la Fuente, F. Sanz-Rodríguez, A. Blazquez-Castro, E. M. Rodriguez, D. Jaque, J. G. Solé, and J. A. Capobianco, "Intracellular imaging of HeLa cells by non-functionalized $NaYF_4$: Er^{3+}, Yb^{3+} upconverting nanoparticles," Nanoscale **2**(4), 495–498 (2010).
28. F. Wang, and X. Liu, "Upconversion multicolor fine-tuning: visible to near-infrared emission from lanthanide-doped $NaYF_4$ nanoparticles," J. Am. Chem. Soc. **130**(17), 5642–5643 (2008).
29. American National Standards Institute, "American National Standard for Safe use of Lasers," (Laser Institute of America, Orlando, FL, 2000).
30. F. Wang, D. Banerjee, Y. Liu, X. Chen, and X. Liu, "Upconversion nanoparticles in biological labeling, imaging, and therapy," Analyst (Lond.) **135**(8), 1839–1854 (2010).
31. F. Wang, and X. G. Liu, "Recent advances in the chemistry of lanthanide-doped upconversion nanocrystals," Chem. Soc. Rev. **38**(4), 976–989 (2009).
32. S. A. Hilderbrand, F. Shao, C. Salthouse, U. Mahmood, and R. Weissleder, "Upconverting luminescent nanomaterials: application to *in vivo* bioimaging," Chem. Commun. (Camb.) (28): 4188–4190 (2009).
33. M. Nyk, R. Kumar, T. Y. Ohulchanskyy, E. J. Bergey, and P. N. Prasad, "High contrast in vitro and in vivo photoluminescence bioimaging using near infrared to near infrared up-conversion in Tm^{3+} and Yb^{3+} doped fluoride nanophosphors," Nano Lett. **8**(11), 3834–3838 (2008).
34. R. A. Farrer, F. L. Butterfield, V. W. Chen, and J. T. Fourkas, "Highly efficient multiphoton-absorption-induced luminescence from gold nanoparticles," Nano Lett. **5**(6), 1139–1142 (2005).
35. G. S. He, K.-T. Yong, Q. Zheng, Y. Sahoo, A. Baev, A. I. Ryasnyanskiy, and P. N. Prasad, "Multi-photon excitation properties of CdSe quantum dots solutions and optical limiting behavior in infrared range," Opt. Express **15**(20), 12818–12833 (2007).
36. It should be mentioned that both two and three power dependences have been reported for upconversion fluorescent gold nanoparticles (see references 9 and 31). Obviously this is related to the participation of different excited states within the involved bands of gold. However, a proper explanation for different observed results does not exist at present.
37. M. Pollnau, D. Gamelin, S. Lüthi, H. Güdel, and M. Hehlen, "Power dependence of upconversion luminescence in lanthanide and transition-metal-ion systems," Phys. Rev. B **61**(5), 3337–3346 (2000).
38. M. A. Albota, C. Xu, and W. W. Webb, "Two-photon fluorescence excitation cross sections of biomolecular probes from 690 to 960 nm," Appl. Opt. **37**(31), 7352–7356 (1998).
39. J. A. Fisher, B. M. Salzberg, and A. G. Yodh, "Near infrared two-photon excitation cross-sections of voltage-sensitive dyes," J. Neurosci. Methods **148**(1), 94–102 (2005).
40. G. Gordillo, F. Rojas, and C. Calderón, "Optical characterization of $Cd(S_x,Te_{1-x})$ thin films deposited by evaporation," Sup. y Vac. **16**, 30–33 (2003).
41. W. R. Zipfel, R. M. Williams, and W. W. Webb, "Nonlinear magic: multiphoton microscopy in the biosciences," Nat. Biotechnol. **21**(11), 1369–1377 (2003).
42. M. D. Leistikow, J. Johansen, A. J. Kettelarij, P. Lodahl, and W. L. Vos, "Size-dependent oscillator strength and quantum efficiency of CdSe quantum dots controlled via the local density of states," Phys. Rev. B **79**(4), 045301 (2009).

#132348 - $15.00 USD Received 27 Jul 2010; revised 24 Sep 2010; accepted 26 Sep 2010; published 26 Oct 2010

1. Introduction

The tremendous advances in nanotechnology together with the availability of non-heating femtosecond near-infrared (NIR) lasers has opened the possibility of realizing whole body *in vivo* fluorescence imaging as an alternative technique to those already in existence (such as proton emission tomography, x-ray computer tomography, and magnetic resonance imaging). Indeed for the implementation of "fluorescence tomography" the development of highly efficient NIR-excited fluorescent nanoparticles (upconverting nanoparticles) is of paramount importance.

In recent years fluorescence bioimaging has shown an impressive development, which has led to intensive research efforts in the field of biophotonics. Although this technique has been traditionally used for *in vitro* imaging and analyte sensing, its use in whole body *in vivo* imaging is still lacking. This is essentially due to the low tissue penetration of the UV/visible optical excitation radiation, high background fluorescence (autofluorescence) and the photodamage of the traditionally used organic probes. Thus, the scientific community has witnessed an impressive growth in the development of an array of luminescent nanoparticles stemming from their versatility in a wide variety of potential applications. The refinement and optimization of their preparation techniques has led to the ability to tailor the nanoparticle and its surface with a high degree of control thus allowing for dispersion in different solvents (including water). Coupled with the particles' nano-size their incorporation in living systems for use as biolabels in fluorescence imaging in various tissues as well as individual cells (including malignant cells) has been realized [1–3]. Many of the fluorescent nanoparticles used as bioprobes for imaging applications rely on single-photon excitation, i.e. excitation *via* short-wavelength light, such as UV or blue, and subsequent emission at longer wavelengths. However, single-photon excitation poses several limitations including the inevitable autofluorescence from other fluorophores in the biological media, as well as low depths of tissue penetration, which hinders their applicability *in vivo*.

To alleviate such issues, nanoparticles that can undergo multiphoton excitation and subsequently emit visible light are currently being investigated [4,5]. Thus, these nanoparticles capable of converting near-infrared (NIR) light to visible, are fast allowing multiphoton excitation fluorescence imaging to become a powerful tool for studying biological functions and offer many advantages over conventional imaging techniques [6,7]. These advantages can be categorized in two different groups, those due to the multiphoton nature of the excitation and those due to the NIR excitation wavelengths. First, as a result of the multiphoton excitation the effective excitation volume with respect to single-photon excitation is reduced thereby allowing for higher spatial resolution [7]. Second, due to the NIR pumping wavelengths, cell damage and autofluorescence are minimized while the tissue penetration depth is enhanced [6]. Traditionally, organic compounds were used as multiphoton excitation fluorescence labels. However, the poor chemical stability of these compounds under high illumination intensities has restricted their real-world application in biological imaging. Thus, interest has shifted towards robust inorganic nanoparticles capable of efficient NIR-to-visible optical conversion by multiphoton excitation.

Perhaps the most well known fluorescent nanoparticles are semiconductor quantum dots (QDs), which are useful as biolabels since their multiphoton excited fluorescence spectra vary depending on the size of the nanoparticle due to the quantum-confinement effect. Thus, the most convenient emission spectrum can be chosen depending on the particular application. It is widely accepted that NIR-to-visible conversion takes place after electronic excitation from the valence to the conduction bands through multiphoton absorption as illustrated in Fig. 1(a), where the dashed lines would represent virtual states within the band-gap. Although they have shown two-photon excited luminescence efficiencies several orders of magnitude larger than those of organic compounds [5], in some cases there are issues related to the relative toxicity of some of their constituent elements (e.g. Cd).

#132348 - $15.00 USD Received 27 Jul 2010; revised 24 Sep 2010; accepted 26 Sep 2010; published 26 Oct 2010

Another well-known class of multiphoton excitation nanoparticles are gold nanorods (GNRs), which show intense visible upconversion fluorescence when excited resonantly at the longitudinal surface plasmon frequency (usually in the NIR), so that high contrast cellular images have been obtained [8–12]. Although mechanisms for the multiphoton excited emission are not trivial, previous works have shown the relevance that the local field enhancement at the surface plasmon frequency together with the participation of electronic states belonging to the *d* and *sp* bands of gold plays in this process [13–16]. These states would correspond to the horizontal solid lines (*d* the lower one and *sp* the upper one) in the diagram in Fig. 1(a) while the horizontal dashed line represents the surface plasmon assistance. Thus, the excitation wavelength for this type of nanoparticle is determined by size/shape effects. Unlike QDs, GNRs have been shown to be relatively non-cytotoxic when appropriately surface functionalized [17].

More recently, a variety of dielectric lanthanide (Ln^{3+})-doped upconverting nanoparticles(UCNPs) have begun to be used as multiphoton excited fluorescent biolabels [18–25]. Typically, the visible fluorescence is generated by the dopant Ln^{3+} ions. The multiphoton mechanism is usually based on an energy transfer between two different Ln^{3+} ions (i.e. Yb^{3+} and Er^{3+} in Fig. 1(b)) [26], which involves a sequential absorption (excitation) of two photons mediated by real electronic states of the donor and acceptor Ln^{3+} ions. The main advantages of UCNPs are their spectral stability, the relatively long lifetime of the electronic states involved in the multiphoton excitation process, and the independence of the fluorescence (excitation/emission) spectra on the particle size. Furthermore, their toxicity has been shown to be significantly lower than that of QDs making them ideal for *in vivo* imaging [18].

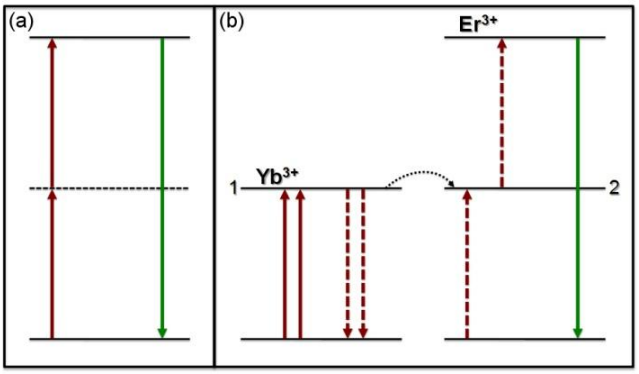

Fig. 1. Schematic excitation flow diagram corresponding to multiphoton excitation (full arrows pointing upwards) in (a) CdSe quantum dots (QDs) and gold nanorods (GNRs) as well as in (b) $NaYF_4$:Er^{3+}, Yb^{3+} nanoparticles (UCNPs). Note: Solid and dashed horizontal lines represent real electronic and virtual states, respectively while the dashed arrows represent a simplified two-step energy transfer process.

2. Experimental

The UCNPs (2 mol% Er^{3+}, 18 mol% Yb^{3+}, respectively) were synthesized via a solvothermal process [27,28]. In a typical experiment, 3.6 mmol of NaCl (99.99%, Aldrich), 1.44 mmol of $YCl_3.6H_2O$ (99.99%, Aldrich), 0.036 mmol of $ErCl_3.6H_2O$ (99.995%, Aldrich), and 0.324 mmol of $YbCl_3.6H_2O$ (99.998%, Aldrich) were dissolved in a 27 mL solution of ethylene glycol (99 + %, Aldrich) containing 0.45 g of branched polyethylenimine (M_w ~25,000, Aldrich) and stirred for approximately 60 min. Subsequently, a solution of 17 mL ethylene glycol with 7.2 mmol NH_4F (99.99 + %, Aldrich) was added to the initial solution containing the chlorides and stirred for another 30 min. The resulting clear solution was then placed in a 250 mL Teflon lined autoclave (Berghof/America) and heated with stirring for 24 h at 200 °C. The resulting nanoparticles were isolated via centrifugation and washed twice with distilled

#132348 - $15.00 USD Received 27 Jul 2010; revised 24 Sep 2010; accepted 26 Sep 2010; published 26 Oct 2010

water and ethanol. The nanoparticles were observed to be quasi-spherical in shape with an average size of 18 nm as determined by transmission electron microscopy (Philips CM200).

The GNRs (Nanopartz TM Inc.) were 45 nm in length and 10 nm in width (i.e. with an aspect ratio of 4.5). The size and shape of these gold nanoparticles determined the longitudinal surface plasmon resonance (circa 830 nm), which lies within the NIR window (700-1000 nm) and so are suitable for deep and safe tissue penetration. The QDs were spherical CdSe nanoparticles of 4 nm in diameter (Invitrogen Inc). Due to their small size these nanoparticles produce a highly efficient two-photon excited fluorescence band centered at approximately 650 nm and also are commonly used for fluorescence bioimaging.

The three types of nanoparticles were each dispersed in PBS (phosphate buffered saline) in concentrations of 1×10^{12}, 0.4×10^{14} and 1×10^{14}nanoparticles per cm^3 for the GNRs, QDs and UCNPs, respectively. These are common concentrations used to obtain reasonable multiphoton excited fluorescence in optical bioimaging experiments at moderate illumination intensities. In all cases, it was verified that at these concentrations the solutions were stable without any evidence of precipitation at room temperature.

The absorption spectra (one-photon absorption) were measured for the three nanoparticle solutions employed in this work by using a double beam UV-VIS-IR spectrometer (Perkin-Elmer Lambda 1050).

The multiphoton excited emission properties of the solutions were studied by placing them in a fiber-coupled fluorescence microscope. A mode-locked Ti:sapphire tunable laser (Tsunami, Spectra Physics) was used as the excitation source. This laser provides 100 fs laser pulses at a repetition rate of 80 MHz as well as the possibility of continuous wave (cw) operation. The laser can be spectrally tuned from 710 to 1000 nm. The NIR laser beam was focused into the solution by using a 10X microscope objective with a numerical aperture (NA) of 0.25. The NIR excitation intensity was controlled by using variable neutral density filters and it was measured by placing a calibrated power meter after the focusing objective. The same objective was used to collect the back-scattered visible fluorescence. After collection, this fluorescence was coupled into a fiber-coupled high-resolution spectrometer equipped with a calibrated diffraction grating and CCD camera.

3. Results and discussion

In order to investigate the viability of using these nanoparticles for highly efficient multiphoton fluorescence imaging and particularly for deep tissue penetration, we have performed a thorough study of their fluorescent properties (excitation, emission and efficiency) and compared them to those of GNRs and QDs biolabels by measuring them under identical experimental conditions. This study was undertaken in a wide excitation intensity range and the obtained results are discussed in terms of the different multiphoton excitation mechanisms. Finally, the excitation spectra of the three nanosystems have been measured in a broad NIR spectral range (700 – 1000 nm) under femtosecond (fs) pulsed laser excitation, the common source in multiphoton fluorescence microscopes. Thus, the working spectral ranges were determined for fs laser excitation for each kind of nanoparticle.

The Ln^{3+}-doped nanoparticles used in this study were $NaYF_4$:Er^{3+}, Yb^{3+} nanocrystals (α-phase) of approximately 20 nm in diameter that were fabricated by a solvothermal synthetic method [27]. This smaller size is ideal to interact with a biological system and to obtain reliable multiphoton fluorescence bioimages. In fact, we have recently demonstrated how these nanoparticles can be used for intracellular imaging [27]. The fluoride host has been shown to be the most ideal to produce the highest NIR-to-visible upconversion efficiency amongst the Ln^{3+}-doped nanoparticles due to their low lattice phonon energies, which minimize the non-radiative decay of the excited states. The pair of optically active Yb^{3+} and Er^{3+} ions was selected because they provide an efficient way of converting the NIR radiation into an intense visible fluorescence by means of an efficient Yb^{3+} to Er^{3+} energy transfer. As

#132348 - $15.00 USD Received 27 Jul 2010; revised 24 Sep 2010; accepted 26 Sep 2010; published 26 Oct 2010

presented in Fig. 1(b), the intermediate levels, denoted as 1 and 2, would correspond to the $^2F_{5/2}$ (Yb^{3+}) and $^4I_{11/2}$ (Er^{3+}) excited energy states.

In order to have a reliable measure of the comparative fluorescence intensity for the three kinds of nano-biolabels, measurements were carried out under identical geometrical configurations and excitation intensities. All the emitted intensities were normalized by the concentration of nanoparticles in the solution leading to what we have defined as the *"Relative Luminescence Signal"*. In this work we explored the multiphoton excited emission in a large range of NIR excitation intensities ranging, from 2 kW/cm^2 to 1 MW/cm^2. This range of excitation intensities is well below the medical safety level (energy density of 100 mJ/cm^2), which in our experimental setup would correspond to an excitation intensity of 8 MW/cm^2 [29].

Figure 2(a) shows the multiphoton excited emission spectra (given as *relative luminescence signal* versus wavelength) and the corresponding photos (right side) obtained from the solutions containing GNRs, QDs and UCNPs as obtained for the maximum excitation intensity achievable in our system (1 MW/cm^2). The excitation wavelengths were tuned to the wavelength at which the emitted signal was at its maximum. More specifically, the wavelengths used were 830, 800 and 980 nm for the GNRs, QDs and UCNPs, respectively. From Fig. 2(a), it is clear that at this excitation intensity the NIR-to-visible optical conversion efficiency of the UCNPs is approximately two times larger than that of the QDs and almost ten times than that of the GNRs. The higher optical conversion efficiency of the UCNPs can be qualitatively explained due to the participation of real electronic states of the Er^{3+} and Yb^{3+} dopant ions in the multiphoton excitation process (see Fig. 1(b)) rather than the virtual states (that possess a much shorter lifetime, and hence a much smaller storage capacity) involved in the multiphoton excitation mechanisms of both GNRs and QDs. It is important to note here that the highest multiphoton relative luminescence signal was observed for the UCNPs not only at this particular excitation intensity but at all the excitation intensities investigated in this work. Finally it should be pointed out that from Fig. 2 it is clear that GNRs, QDs and UCNPs show an appreciable visible emission under NIR excitation when spatially localized at focus. These two facts indicate that all the nanoparticles under study in this work can be used as two-photon contrast agents as it has been already demonstrated for both *in vivo* and *in vitro* experiments [30,31].

#132348 - $15.00 USD Received 27 Jul 2010; revised 24 Sep 2010; accepted 26 Sep 2010; published 26 Oct 2010

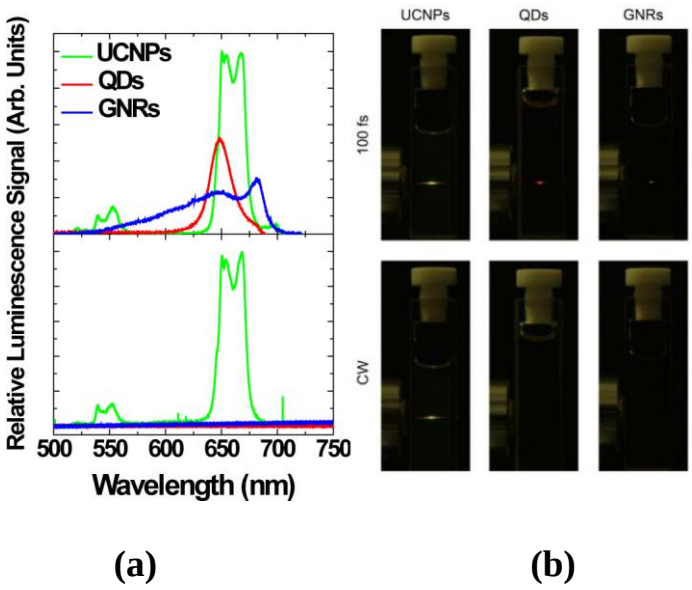

Fig. 2. *Left Side.* (a) Multiphoton relative luminescence signal generated by the QD, GNR, and UCNP solution as obtained under fs laser excitation at 800, 830 and 980 nm, respectively. Pump intensity was 1 MW/cm^2. (b) Multiphoton relative luminescence signal generated by the QD, GNR, and UCNP solution as obtained under cw laser excitation at 800, 830 and 980 nm, respectively. Pump intensity was 1 MW/cm^2. *Right Side.* Photos corresponding to the naked eye observations of the fluorescent samples in Fig. 2(a), upper photos, and Fig. 2(b), bottom photos. The pump intensity was kept the same in both cases (CW and 100 fs excitation)

Figure 3(a) shows the relative NIR-to-visible relative luminescence signal for the GNRs, QDs and UCNPs as a function of the excitation intensity. At all excitation intensities the relative emission luminescence signal generated by the UCNPs was larger than those generated by GNRs and QDs. More importantly, it should be noted that for lower excitation intensities the differences in the conversion efficiencies are quite remarkable, however, as the excitation intensity is increased these differences are significantly lower.

The data presented in Fig. 2(a) and 3(a) were obtained using a Ti:sapphire laser working in the pulsed (mode-locking) regime. However, when the nanoparticles were excited with the Ti:sapphire working in continuous wave (cw) mode at identical average excitation intensities, multiphoton excited emission was only observed from the solution containing the UCNPs (see Fig. 2(b) and corresponding photos on the right). Clearly, this fact indicates that both the QDs and GNRs require very high photon densities for multiphoton excitation whereas the key parameter for the UCNPs is the average incident photon flux. This can be again explained in terms of the role played by the real electronic states in the multiphoton excitation of the UCNPs. The lifetime of these electronic real states (in the order of μs) is much longer than the pulse duration so that the number of excited electrons does not depend on the peak photon intensity but on the average photon flux. This is an important advantage of UCNPs over QDs and GNRs since it means that inexpensive and readily available continuous wave excitation beams can be used for multiphoton excited cell imaging [32,33].

#132348 - $15.00 USD Received 27 Jul 2010; revised 24 Sep 2010; accepted 26 Sep 2010; published 26 Oct 2010

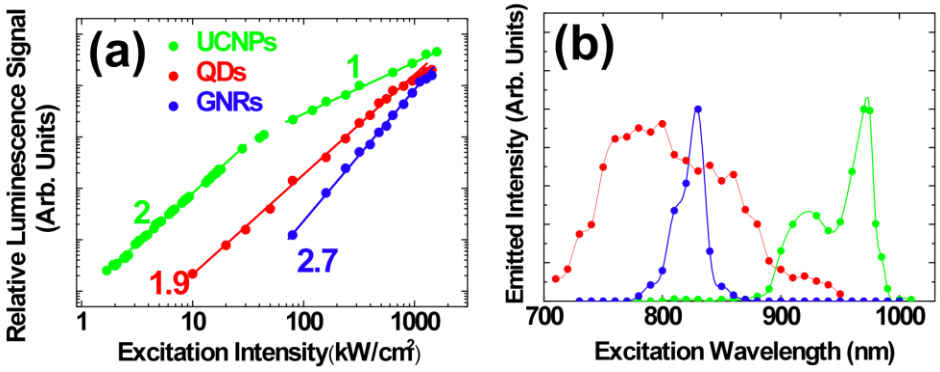

Fig. 3. (a) Relative luminescence signal of QDs, GNRs, and UCNPs as a function of fs excitation intensity. (b) Excitation spectra of the multiphoton excited fluorescence for QDs, GNRs, and UCNPs. Pump intensity was 20 kW/cm^2. Note: The excitation wavelengths used in Fig. 3(a) correspond to the peak maxima in the excitation spectra (Fig. 3(b)).

An important aspect related to multiphoton imaging is the investigation of the photon-order excitation dependence and how it is affected by the excitation intensities. We have observed different dependencies of the fluorescence signal with the multiphoton excitation power (intensity) for each system. GNRs and QDs show monotonic power dependencies and the slopes in the double-logarithmic representation have been found to be 2.7 and 1.9, respectively (see Fig. 3(a)). The power dependence observed for QDs is in good agreement with previous works and is consistent with a two-photon excitation process while the observed behavior for GNRs is closer to a three-photon excitation process [34–36]. On the other hand, the UCNPs showed two clear distinct regimes where at low excitation intensities (<60 kW/cm^2) the visible fluorescence follows a quadratic dependence (as initially expected for a two-photon excitation process). For high excitation intensities (>60 kW/cm^2) this dependence becomes linear. This result occurs as a consequence of the increasing competition between linear decay and upconversion for the depletion of the intermediate excited states [37]. The presence of these two excitation regimes in the multiphoton excited fluorescence of UCNPs makes the excitation intensity an important parameter when designing bioimaging experiments of high spatial resolution based on UCNPs. In fact, to take advantage of the spatial resolution enhancement induced by multiphoton excitation, the excitation intensity should lie in the quadratic regime; i.e. not exceeding 60 kW/cm^2. This is clearly observed in the photos in Fig. 2, where the spatial resolution is lower for the UCNPs than for the QDs and GNRs due to the high excitation intensity used, which excites the UCNPs in the linear regime. As it is discussed next, the presence of saturation in the two-photon process (that results in the linear behavior) also has a strong relevance when the two-photon excitation volume is calculated.

At this point, we can use our experimental data to obtain specific values for the multiphoton excited fluorescence efficiency of the UCNPs. Recall here that because the upconversion process is non-linear, the efficiency is dependent on both the excitation intensity and the excitation power dependence regime. At moderate excitation intensities (kW/cm^2) it is clear that both QDs and UCNPs follow a quasi-quadratic behavior. In these conditions the relative intensities can be used to compare the so-called "two-photon action cross-section" (Θ_2) of QDs and UCNPs. This parameter is defined as the product of the two-photon absorption cross-section per nanoparticle (σ_2) and the fluorescence quantum efficiency (Φ_f), such that $\Theta_2 = \Phi_f \cdot \sigma_2$ provides a direct measure of brightness [7]. Under equal excitation conditions (intensity and pulse length) the ratio between the two-photon action cross-sections

#132348 - $15.00 USD Received 27 Jul 2010; revised 24 Sep 2010; accepted 26 Sep 2010; published 26 Oct 2010

of QDs and UCNPs can be experimentally obtained from the ratio of their emitted intensities [38,39]:

$$\frac{\Theta_2^{QD}}{\Theta_2^{UCNP}} = \frac{I_2^{QD}}{I_2^{UCNP}} \cdot \frac{n_{QD}}{n_{UCNP}} \quad (1)$$

where I_2^{QD} / I_2^{UCNP} is the ratio between the (two-photon excited) emitted intensities per nanoparticle (QD or UCNP), and n_{QD} ≈2.3 and n_{UCNP} ≈1.8 are the real part of the linear refractive index at the excitation wavelengths for QDs and UCNPs, respectively [40]. The evaluation of I_2^{QD} / I_2^{UCNP} requires the knowledge of the two-photon intensities emitted per QD and per UCNP and, hence, the knowledge of the two-photon excitation volume, V_2^{exc}. This can be calculated from the concentration of solutions (nanoparticles per unit volume) by multiplying it by the effective two-photon excitation volume (V_2^{exc}). According to previous works, and taking into account the numerical aperture of the microscope objective used in this work V_2^{exc} is given by [41]:

$$V_2^{exc} = 0.5 \cdot \frac{\lambda^3}{NA^2} \cdot \left[\frac{1}{n - \sqrt{n^2 - NA^2}} \right] \quad (2)$$

where NA is the numerical aperture of the focusing optics (0.25), λ is the pump wavelength and *n* is the refractive index of the solution (assumed to be 1.3). According to expression (2) we have obtained a two-photon excitation volume of ≈170 and ≈300femto-liters for QDs and UCNPs, respectively. Note that expression (2) is only valid in absence of saturation effects in the two-photon luminescence. Therefore, the excitation volumes estimated here can only be applied (in the case of UCNPs) for excitation intensities below 60 kW/cm^2 (see Fig. 3(a)). Taking into account these volumes and the concentration (in nanoparticles per unit volume) as well as the data of Fig. 3(a) we have found I_2^{QD} / I_2^{UCNP} ≈0.05 at 20 kW/cm^2 of excitation intensity. Thus, from expression (1), we obtain, Θ_2^{UCNP} ≈16 x Θ_2^{QD} i.e. the two-photon action cross section of a single UCNP is more than one order of magnitude than that of a single QD. Both the fluorescence quantum efficiency and the two-photon cross-section per QD have been estimated previously for CdSe QDs of similar size to the ones used in this work. The obtained values were determined to be Φ_f = 0.7 and σ_2 = 2.4 x 10^{-20} cm^4/GW (per quantum dot) [35,42], which results in Θ_2^{QD} ≈1.68 x 10^{-20} cm^4/GW, i.e. 4 x 10^2 GM units (being the two-photon cross section defined per quantum dots). Now, using this value and Eq. (1) we can calculate the two-photon action cross-section (per UCNP) to be Θ_2^{UCNP} ≈2.7 x 10^{-19} cm^4/GW, i.e. 5 x 10^3 GM units (per nanocrystal). To the best of our knowledge, this is the first time that this value has been reported for UCNPs. The comparison of this spectroscopic parameter with that of GNRs is not possible since unfortunately, they do not show the same two-photon power dependence as QDs and UCNPs (see Fig. 3(a)). Finally it is important to highlight that the obtained values of the two-photon action cross sections are only valid for these specific particle sizes which as previously commented are the most common ones for biological multi-photon fluorescence imaging.

To glean information on the working wavelength range of the UCNPs and how it compares to those of the commercial nano-biolabels, the excitation spectra of GNRs, QDs and UCNPs were also measured by tuning the fs laser excitation wavelength, from 710 to 1000 nm and the results are shown in Fig. 3(b). It can be seen that the emission of UCNPs can be efficiently multiphoton excited in a wide spectral range (900-990 nm). This excitation range shows a partial spectral overlap with the water absorption band (relevant above 950 nm). This

#132348 - $15.00 USD Received 27 Jul 2010; revised 24 Sep 2010; accepted 26 Sep 2010; published 26 Oct 2010

fact allows for the acquisition of multiphoton excited fluorescence images of biological systems in the presence or absence of pump induced heating due to water absorption. It should be noted that the spectral excitation working range of the UCNPs is different than that of the QDs (710-950 nm) and the GNRs (only efficient around the longitudinal surface plasmon frequency).

Finally, it should be noted that from the one-photon absorption spectra of the three solutions we have evaluated the one-photon absorption coefficients at those wavelengths leading to optimum excitation in each case: 800, 825 and 975 nm for QDs, GNRs and UCNPs, respectively. The one-photon absorption coefficients (α_{abs}) were found to be <0.02, ≈3 and <0.02 cm^{-1} for QDs, GNRs and UCNPs solutions, respectively. These one-photon absorption coefficients lead to absorption lengths ($l_{abs}\approx 1/\alpha_{abs}$) in the order of tens of centimeters for QDs and UCNPs and close to 3 mm in the case of GNR. Thus, both QDs and UCNPs would be more appropriate than GNRs in those bio-imaging applications requiring large penetration depths. It should be noted that although real electronic states are involved in the two-photon emission of UCNPs, the typical low absorption cross sections of lanthanides, the relatively low doping level (≈0.2) of absorption centers (lanthanide ions) in the nanoparticles and the low concentration of nanoparticles in the solution makes the one-photon absorption of the UCNPs negligible.

4. Conclusion

In summary, we have demonstrated for the first time that fluoride-based inorganic upconverting nanoparticles, $NaYF_4:Er^{3+}$, Yb^{3+}, are the most efficient multiphoton excited fluorescent nanoparticles developed to date. The efficiency of the aforementioned nanoparticles clearly surpasses that of quantum dots and gold nanorods, which are the commercially available inorganic fluorescent nanoprobes presently used for multiphoton fluorescence bioimaging. Thus, the $NaYF_4:Er^{3+}$, Yb^{3+} UCNPs display the largest relative multiphoton excited upconversion fluorescence efficiencies at all the investigated fs laser excitation intensities (from 1 to 1000 kW/cm^2). This larger relative efficiency is still favored for low and moderately low excitation intensities (1 to 12 kW/cm^2), so that only these nanoparticles are capable of multiphoton emission under continuous wave excitation. This superior NIR-to-visible conversion efficiency, mostly due the assistance of real electronic states during the multiphoton excitation process, makes these nanoparticles very promising for highly efficient multiphoton fluorescence imaging, providing the possibility of using simple and inexpensive cw lasers. In addition, these nanoparticles open new perspectives for the actual development of *in vivo* fluorescence tomography imaging. The broad excitation spectra of these nanoparticles provide the possibility of wavelength tuning to the most convenient range for a particular application.

Acknowledgements

This work was supported by the Universidad Autónoma de Madrid and Comunidad Autonoma de Madrid (Projects CCG087-UAM/MAT-4434 and S2009/MAT- 1756), by the Spanish Ministerio de Educacion y Ciencia (MAT 2007-64686), and by a Banco Santander-CEAL-UAM project. The authors also thank the Natural Sciences and Engineering Research Council (NSERC) of Canada and the Gouvernement du Québec, Ministère du Développement économique, de l'Innovation et de l'Exportation for funding. E. Martin Rodriguez is supported by the Spanish Ministry of Education (FPU program, ref. AP2006-02795). J.G.S. thanks the Spanish Minsterio de Educación for financial support for a research stay at Concordia University (ref PR2009-0040).

#132348 - $15.00 USD Received 27 Jul 2010; revised 24 Sep 2010; accepted 26 Sep 2010; published 26 Oct 2010